

# Variability of stratification and currents at the submesoscale detected from CTD and current profiles in the central Gulf of Finland

Madis-Jaak Lilover\*, Urmas Lips, Taavi Liblik, Irina Suhhova and Germo Väli

*Department of Marine Systems, Tallinn University of Technology, Tallinn, Estonia*  
*\*corresponding author's e-mail: madis.lilover@taltech.ee*

*Received 17 Jun. 2024, final version received 10 Feb. 2025, accepted 10 Feb. 2025*

Lilover M.-J., Lips U., Liblik T., Suhhova I. & Väli G. 2025: Variability of stratification and currents at the submesoscale detected from CTD and current profiles in the central Gulf of Finland. *Boreal Env. Res.* 30: 77–92.

This study investigates submesoscale variability in the Gulf of Finland resulting from atmospheric forcing on estuarine hydrographic gradients. Utilizing autonomous vertical profilers, we observed upwelling/downwelling events, their relaxation, and accompanying high-frequency variability. The temperature variance spectrum at isopycnal surfaces exhibited a slope of  $-2$ , a characteristic sign of active submesoscale (SMS) processes. The footprints of SMS processes were observed at the deep thalweg station during the upwelling relaxation period. In the thermocline, intensified high-frequency temperature fluctuations coincided with the changes in velocity and salinity. Observations at the shallow station revealed temperature and salinity fluctuations likely linked to SMS processes during the downwelling relaxation event under calm weather conditions. Approximately 50% of the observed high-frequency temperature variability (temperature fluctuations ranging from  $-1.2$  to  $1.8^{\circ}\text{C}$ ) was explained by SMS processes, while the remaining 50% resulted from vertical excursions of isopycnals. This result indicates that SMS processes are potentially significant in the gulf's dynamics.

## Introduction

Mesoscale eddies play a fundamental role in ocean dynamics, serving as key drivers for transporting heat, momentum, and various tracers (nutrients, pollutants, etc.) over significant spatial scales (Holland 1978). Mesoscale eddies formed due to the baroclinic instability of boundary currents and frontal zones convert potential energy into kinetic energy, facilitating energy transfer from large-scale oceanic gyres to smaller scales (Gill *et al.* 1974; Levy *et al.* 2018). While the variability of oceanographic

fields at the mesoscale and larger scales is well-documented, the energy transfer pathways to the submesoscale and the subsequent dissipation remain incompletely understood.

Submesoscale currents, characterized by horizontal scales of 0.1–10 km, exhibit order-one Rossby ( $Ro$ ), internal Froude ( $Fr$ ), and balanced Richardson ( $Ri_b$ ) numbers (Thomas *et al.* 2008; McWilliams 2016). These structures manifest as density fronts, filaments, topographic wakes, and coherent vortices at the surface and throughout the ocean interior. Submesoscale motions are crucial in directing energy from mesoscale



**Fig 1.** Satellite image depicts the inhomogeneities of the cyanobacterial bloom at the small scales (Northern Baltic Proper, the entrance area of the Gulf of Finland, 8 August 2022, European Union, Copernicus Sentinel-2 imagery — processed by @DEFIS\_Eu). The size of the image is about 90 x 50 km, and the location of the photo is depicted in Fig. 2.

(balanced) flows towards microscale dissipation and diapycnal mixing (McWilliams 2016). The preconditions for intensified sub-mesoscale processes involve strong lateral buoyancy gradients, strong vertical vorticity, and weak vertical stratification (Thompson *et al.* 2016). The characteristic time scales of sub-mesoscale motions range from hours to days, overlapping with the time scales of inertia-gravity waves (IGW), necessitating differentiation between these two classes of motions (McWilliams 2016).

Research on energetic wintertime sub-mesoscale turbulence indicates that wavelengths of approximately 10 km correspond to time scales of about one day, emphasizing that sub-mesoscale turbulence evolves on time scales comparable to or shorter than the inertial period (Callies *et al.* 2020). The transition from mesoscale to submesoscale is quantitatively associated with the first baroclinic Rossby radius of deformation (Thomas *et al.* 2013; Zhang *et al.* 2020). A departure from geostrophically balanced dynamics ( $Ro \sim 1$ ) implies the development of ageostrophic circulation patterns characterized by higher vertical velocities (Molemaker *et al.* 2010; Sullivan and McWilliams 2018).

Submesoscale structures play a pivotal role in ocean dynamics, particularly when influenced by energetic mesoscale flow fields (Thomas *et al.* 2008; Capet *et al.* 2008; Gula *et al.* 2014). These structures, such as frontogenesis and filamentogenesis, are often associated with strong horizontal density differences and ambient strain

flows provided by mesoscale currents and eddies (Capet *et al.* 2008; Gula *et al.* 2014).

The Gulf of Finland, spanning approximately 400 km in length and 48–135 km in width, features a complex circulation pattern influenced by its variable coastline, bottom topography, and significant salinity gradients. Large freshwater input from the river Neva and saline water inflow from the Baltic Proper create pronounced along-axis surface salinity variations, ranging from  $7 \text{ g kg}^{-1}$  at the deep entrance (depth of about 100 m) to  $3 \text{ g kg}^{-1}$  at the shallow eastern end (depth of about 20 m) (Alenius *et al.* 1998). A quasi-permanent halocline at about 60 to 80 meters separates the deep layer with a salinity of  $8\text{--}11 \text{ g kg}^{-1}$  from the upper layer in the western part and further contributes to the intricate circulation dynamics. Salinity variations in the whole water column are strongly influenced by the seasonality of atmospheric forcing and riverine freshwater input (Haapala and Alenius 1994; Liblik and Lips 2012). The current structure of the gulf is layered and variable and strongly linked to the seasonal thermocline and halocline (e.g. Lilover *et al.* 2017; Suhhova *et al.* 2018). Therefore, the Gulf of Finland, an elongated estuarine-like sub-basin of the Baltic Sea, offers an ideal setting for studying submesoscale processes due to its unique characteristics, including strong horizontal and vertical water density and current velocity gradients.

Observations in the Baltic Sea have identified submesoscale eddies (5–20 km in diameter) under moderate and calm wind conditions (Gurova and Chubarenko 2012; Karimova and Gade 2016). Satellite-based studies utilizing SAR images revealed the prevalence of submesoscale eddies, particularly in regions of sharp shear changes and surface temperature fronts (Tavri *et al.* 2016). For example, in Fig.1, the small-scale inhomogeneities of the cyanobacterial bloom in the Gulf of Finland are shown (ESA Copernicus, Sentinel-2, 8 August 2022). Additionally, high-resolution modelling has contributed valuable insights into submesoscale structures; cyclonic structures, vortices, and spiral eddies have been detected in simulations during specific phases of upwelling events (Väli *et al.* 2017 and 2018; Zhurbas *et al.* 2021). Similarly, Chrysagi *et al.* (2021) confirmed that

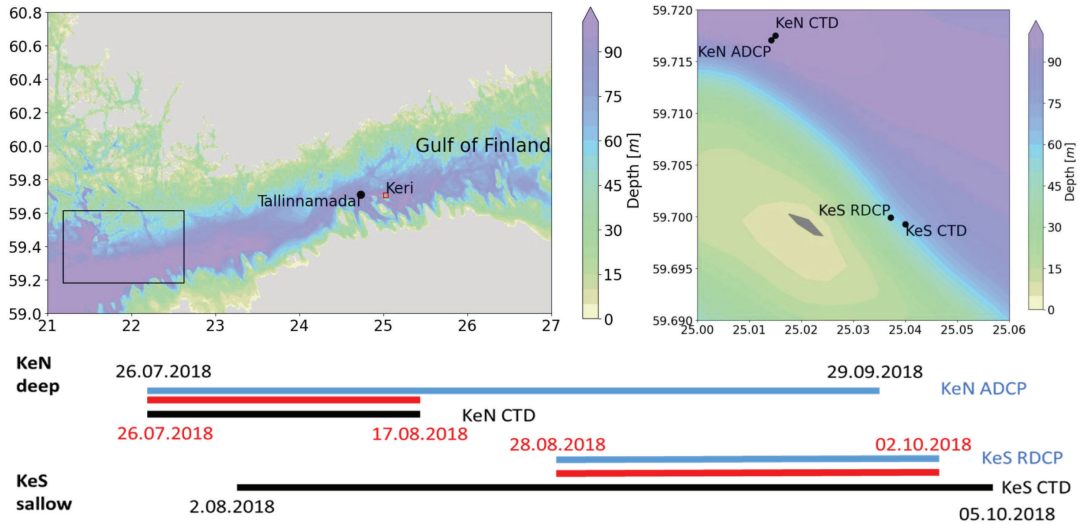


**Fig 2.** Bathymetry and locations of the autonomous CTD profilers and bottom-mounted ADCP and RDCP close to Keri Island in the Gulf of Finland (red square, black dots). The location of the Tallinnamadal weather station is shown by a black dot in the left panel. The black rectangle marks the area covered by the photo in Fig. 1. The schema in Fig. 2 depicts the time windows of measurements at KeN and KeS stations (the blue line corresponds to ADCP measurements, the black line to CTD and the red line shows the time window for coinciding measurements by ADCP and CTD).

submesoscale processes can maintain a shallow mixed layer during storms and induce rapid restratification afterwards. Submesoscale features are inhomogeneously distributed in the Baltic Sea; besides the eastern region of the Gotland Basin mentioned by Chrysagi *et al.* (2021), they occur more frequently in the Gulf of Finland (Väli *et al.* 2024). Field studies in the Gulf of Finland have highlighted the importance of submesoscale processes in energy cascades to smaller scales (Lips *et al.* 2016). The recent observations suggest that submesoscale structures are strongly connected to the mesoscale flow field (Salm *et al.* 2023). The presence of sub-mesoscale processes has been linked to diverse phenomena, including salinity inversions, coastal upwelling, and the generation of plankton patches (Lips *et al.* 2016; Burchard *et al.* 2017; Pietri *et al.* 2013). Understanding the origin and impact of these submesoscale features on oceanic biodiversity remains a critical challenge.

High-resolution in situ measurements in space (horizontal step of a few hundred meters or less) and/or time (time step less than a few hours) are required to reveal submesoscale features. In the present study, we characterize sub-

mesoscale variability based on high-frequency vertical profiles of currents, temperature and salinity at fixed locations in the Gulf of Finland. We aim to show the occurrence of submesoscale processes, distinct from internal waves (IW), in the context of larger-scale hydrographic background and variability. We suggest that energetic submesoscale events could occur with mesoscale coastal upwelling/downwelling development and relaxation.

Following a description of the material and methods used, we present the analysis of background mesoscale phenomena, indicators of submesoscale processes, and the emergence of energetic submesoscale events. Finally, discussion and conclusions are presented.

## Material and methods

### Oceanographic field measurements

Oceanographic measurements, encompassing currents, water temperature, and salinity, were conducted at two proximate locations near Keri Island (Fig. 2, Table 1). The bottom-mounted ADCP (Acoustic Doppler Current Profiler,

Workhorse Sentinel, Teledyne RDI, 300 kHz) measured current profiles for two months, from August to September 2018, at the KeN measurement station, approximately 2 km north of Keri Island. Simultaneously, temperature and salinity profiles were recorded for nearly one month by a bottom-mounted autonomous CTD profiler (Flydog Solutions) at the KeN from 26 July 2018 to 17 August 2018. CTD (Conductivity, Temperature, Depth) profiles were recorded from 3 to 98 meters at 3-hour intervals and ADCP data at 5-minute intervals from 8 to 106 meters. The horizontal separation between the locations of CTD and ADCP profilers was 60 m.

The bottom-mounted RDCP (Recording Doppler Current Meter, Aanderaa Data Instruments AS) measured current profiles for one month, spanning from 28 August to 2 October 2018, at the KeS measurement station, approximately 1.1 km east of the island. Simultaneously, temperature and salinity profiles were obtained for two months by a buoy-mounted automatic CTD profiler (Idronaut) at the KeS from 28 August 2018 to 5 October 2018. CTD data, available at 6-hour intervals, covered depths from 2 to 44 meters, and RDCP data, recorded every 30 minutes, spanned depths from 6.8 to 42 meters. The separation between the locations of CTD and RDCP profilers was 300 m.

Despite the proximity of approximately 2.5 km between KeN and KeS stations, their locations played a crucial role in observations. Namely, KeN was situated on the thalweg of the Gulf of Finland, while KeS was in a shallower area shadowed by Keri Island from the west.

High-resolution wind data for the measurement period were obtained from the Tallinnamadal Lighthouse, about 20 km west of the measurement site. Wind speed and direction

sensors (Aanderaa) at a height of 31 m recorded data every 5 minutes.

The rotary spectra analysis of current velocity raw data identified white noise at time scales of less than two hours. A low-pass Butterworth filter with a 2-hour cutoff was applied to the current profiles' time series, resulting in a white noise-free filtered time series with a time step of 1 hour.

### Separating submesoscale from mesoscale

Let  $L$  be a characteristic length and  $U$  a characteristic horizontal velocity scale, then  $L/U$  gives the characteristic time scale of motions. If the Rossby number

$$Ro \equiv U/Lf = 1, \quad (1)$$

(where  $f$  is the Coriolis parameter), the characteristic time scale of motions equals the local inertial period, which is approximately 14 hours in the Gulf of Finland. Model simulations have revealed small eddies and structures with Rossby numbers equal to 2 or higher (Väli *et al.* 2017; Zhurbas *et al.* 2021), indicating their characteristic time scales 7 hours or less (at our latitudes). Although no strict upper limit of the lifetime of the submesoscales (e.g. submesoscale coherent vortices) can be defined, the SMS range from hours to days is usually considered (McWilliams 2016).

Current velocity spectra calculated from ADCP and RDCP data at stations KeN and KeS for the surface layer revealed energy minima at a frequency corresponding to the time scale of 36 hours. The spectra showed elevated kinetic energy at higher frequencies (HF, high-frequency

**Table 1.** Information on the conducted measurements.

Keri Island	Measurement period	Duration	59°41.95' North	25°1.27' East	Depth
KeN currents	26.07.2018–29.09.2018	10 weeks	59° 43.025'	25° 0.855'	110m
KeN CTD	26.07.2018–17.08.2018	3 weeks	59° 43.050'	25° 0.900'	110m
KeS currents	28.08.2018–02.10.2018	5 weeks	59° 41.994'	25° 2.231'	46m
KeS CTD	02.08.2018–05.10.2018	9 weeks	59° 41.958'	25° 2.406'	46m

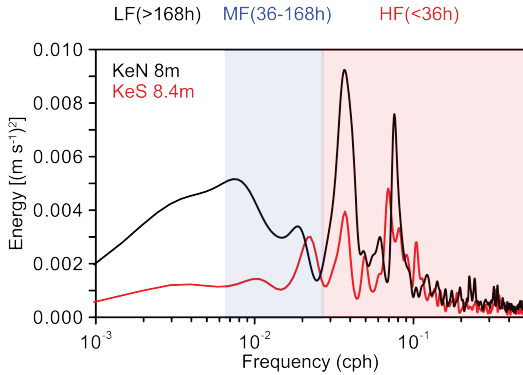


**Fig 3.** Current velocity energy spectra from ADCP and RDCP data at stations KeN and KeS for the surface layer. The semi-transparent red vertical rectangle marks timescales 2–36 hours and blue timescales 36–168 hours.

band, time scales from 36 to 2 hours), and some peak values of kinetic energy were observed at medium frequencies (MF band, time scales from 36 hours to 168 hours) (Fig. 3).

Following the rationale above we decomposed using low-pass Butterworth filter the measured velocity components  $u$  and  $v$ , and temperature,  $T$ , salinity,  $S$ , and water density,  $\sigma_0$ , into three distinct frequency bands in the following way:

$$u = u_{LF} + u_{MF} + u_{HF}; v = v_{LF} + v_{MF} + v_{HF};$$

$$T = T_{LF} + T_{MF} + T_{HF}; S = S_{LF} + S_{MF} + S_{HF}, \quad (2)$$

where LF marks timescales  $> 168$ h, MF timescales 36–168h, and HF timescales  $< 36$ h. In the present study, we discuss these frequency bands separately, aiming to discern the submesoscale dynamics.

It is important to note that the high-frequency part of motions contains not only the signal of submesoscale processes but also inertial, tidal, and seiche-related contributions. The latter processes cause variations in the vertical location of the isopycnal surfaces, while the properties of water parcels moving with isopycnals do not change considerably in case of no mixing. To highlight the submesoscale signal within the HF band, the influence of vertical oscillations and movements of isopycnals (e.g. due to upwellings and downwellings) should be eliminated. This can be done by presenting the variability of tem-

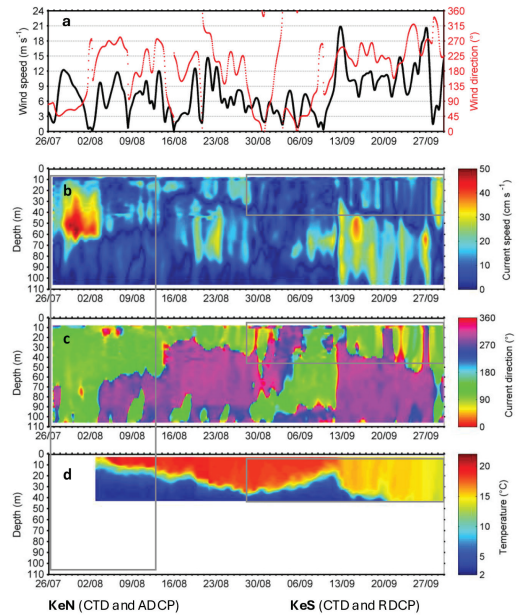


**Fig 4.** Temporal course of the low pass filtered (36 h) (a) wind speed and direction at Tallinnamadal meteorological station, (b, c) current velocity speed and direction in the water column at measurement station KeN and (d) water temperature at measurement station KeS. The grey rectangles mark the time windows of current and CTD measurements at both stations. A detailed description of CTD and current fields in these time windows is given in Fig. 5.

perature and salinity at isopycnal surfaces. The applicability of the approach is confirmed by the distribution of spectral density of isopycnic temperature variations, which does not show peaks at any frequencies (including the frequency of inertial oscillations) and will be discussed below.

## Results

### Basics of the wind and current

#### Wind

Throughout the two-month measurement period, prevailing winds were predominantly either from the SW or NE sectors, specifically within the sectors of 236 to 260 degrees and 45 to 68 degrees (Fig. 4a). The wind speed exhibited moderate variability, dropping below  $3 \text{ m s}^{-1}$  for 17 days and exceeding  $10 \text{ m s}^{-1}$

for approximately 19 days. Notably, two strong wind events, each lasting about one day with speeds surpassing  $15 \text{ m s}^{-1}$  were recorded on September 12 and 26. Westerly winds dominated the observation period, marked by extended periods lasting 3 to 11 days (August 3–7, August 11–13, August 18–27, August 30–September 4, and September 11–20). However, two longer intervals (July 27–August 1 and August 28–September 8) experienced easterly winds. Only three instances featured stronger northerly winds. The observation period unfolded as a sequence of alternating upwelling- and downwelling-supporting wind periods: a 5-day easterly wind period transitioned to a 14-day westerly wind period, reverted to easterly winds for 11 days, and then resumed westerly winds for 24 days, including brief wind ceasing periods in the final ten days.

### Current and water temperature structure

Two or three-layer vertical current structures were observed at the KeN during the study period. (Fig. 4b, c). The upper layer current generally aligned with the wind vector, while the layer below exhibited a counter-wind direction. The upper mixed layer depth gradually changed from an initial 10 m to 60 m by the end of the measurements. Periodically, a third layer, with a low current speed beneath the halocline (around 70 m), developed for shorter periods (1–4 days) and followed the local bottom topography, changing from NW to SE every 3–4 days. Instances of a one-layer current structure were noted three times: on 3 August, when the top layer diminished, and on 21 and 27 September, when the uppermost layer extended to at least 40 meters and briefly changed direction. Strong currents occurred in the cold intermediate layer, particularly until 13 September, after which strong currents also occupied the lower layer. These currents were directed eastward during easterly winds and westward during westerly winds, effectively opposing the wind. An exceptionally robust eastward current, lasting one week (up to  $0.7 \text{ m s}^{-1}$ ), was observed during the first easterly wind period (26 July–2 August). The water temperature in the upper 40 meters

recorded at KeS station showed the alternations of upwelling, upwelling relaxation, downwelling, downwelling relaxation, and again downwelling according to the wind and currents events (Fig. 4d).

## Mesoscale phenomena

### Mesoscale phenomena at KeN station (CTD and currents)

During the three-week co-measurements at KeN station, a dynamic sequence unfolded. Initially, an about one-week upwelling phase was observed, succeeded by one week of upwelling relaxation, and ultimately transitioning into a downwelling period (Fig. 5). The observed temperature patterns were influenced by preceding east wind events, with the upwelling raising the cold intermediate layer, resulting in a temperature drop to 6 degrees at 10 m depth. Subsequently, a very strong wind impulse from the east supported upwelling, causing the thermocline (15-degree isoline) to rise to the surface while maintaining the cold intermediate layer at 20 m depth. The observed southward current component below the Ekman layer confirmed the subsurface circulation in accordance with the upwelling development (Fig. 5f). Over the next two weeks, the impact of the westerly wind supporting downwelling became evident, leading to the thickening and re-establishment of the warmer surface layer. Concurrently, variable eastward wind stress dominated, contributing to a wind impulse change from  $-0.43$  to  $0.12 \text{ N m}^{-2}$  between 3 and 14 August. Salinity variations mirrored temperature changes, with cold water exhibiting higher salinity. The upwelling and downwelling effects were confined to the uppermost 30 m layer. Water density ( $\sigma_0$ ) followed water temperature and salinity, varying significantly at 10 and 20-meter depths, from 2 to 4.5 and 4.5 to 5.5  $\text{kg m}^{-3}$ , respectively. Buoyancy frequency square ( $N^2$ ), a key indicator of density stratification, effectively traces the evolution of the upper mixed layer, the thermocline and the halocline. Vertical gradients of currents and buoyancy (expressed as the square of current velocity shear ( $s^2$ ) and the buoyancy frequency

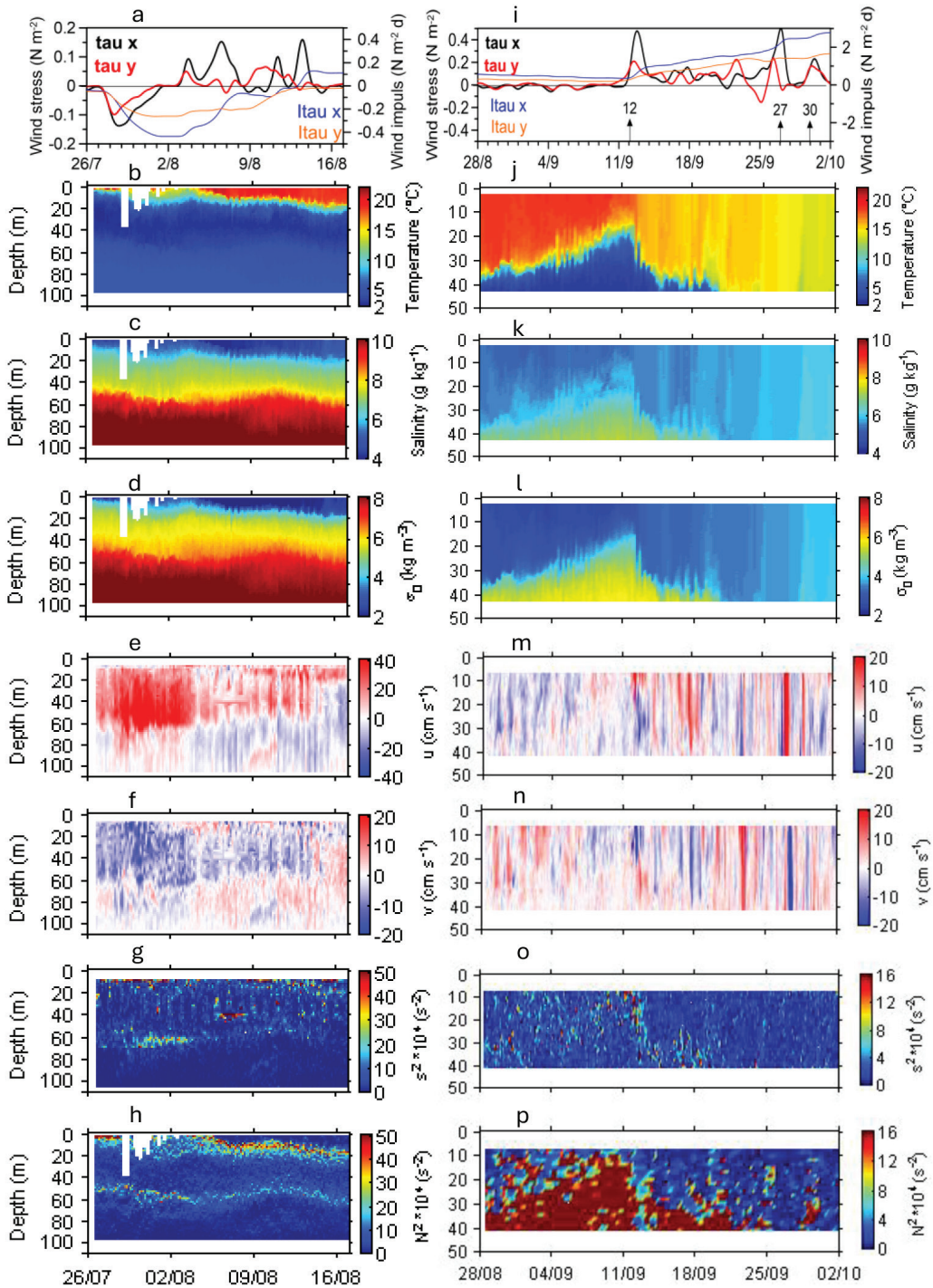


**Fig 5.** Wind stress and wind impulse components together with temporal evolution of temperature, salinity, density, current  $u$ - and  $v$ -components,  $s^2$  and  $N^2$  for the periods of parallel CTD and current measurements at KeN station (left column) and KeS station (right column). Arrows and numbers in Fig. 5i depict the strong wind events in September (note that wind stress has different scaling in panels (i) and (a)). The halocline vertical position is seen in panel (c) as the starting depth of the red colour.

square) agreed well in the thermocline, which was re-established during the second half of measurements), and in the halocline, particularly during the first half of measurements (Fig. 5g, h).

### Mesoscale phenomena at KeS station (CTD and currents)

The period of parallel CTD and current measurements at KeS station extended over five weeks, characterized by two weeks of downwelling relaxation followed by three weeks of sustained downwelling, interspersed with three successive stormy wind events (Fig. 5). The initial downwelling relaxation was associated with relatively weak wind stress, causing a gradual decrease in the thickness of the warm upper mixed layer from 35 m to 15 m. Northward velocity in the upper layer supported restratification of the upper 30 m layer. A strong westerly wind event on 12 September led to a new mixed layer and a deeper thermocline. After the wind event, downwelling-supporting wind impulses increased to  $1.16 \text{ N m}^{-2} \text{ d}$  during the event and continued to rise to  $2.31 \text{ N m}^{-2} \text{ d}$  over the next 10 days. Another extreme west wind event on 27 September resulted in the vertical mixing and cooling of the upper layer, featuring a strong single-layer current. At the end of this wind event, a relatively weak thermocline recovered at a depth of 30 meters. However, a new westerly wind event on 30 September destroyed the thermocline, causing the depth of the upper mixed layer to reach at least 44 meters. Similar to the measurements at the KeN station, the square of current velocity shear ( $s^2$ ) exhibits a noteworthy correlation with the buoyancy frequency square (Fig. 5o, p). The concurrent behaviour of  $N^2$  and  $s^2$  was previously noted by Suhhova *et al.* (2018) in the Gulf of Finland.

### Scale-dependent distributions of kinetic energy, shear, and water density fluctuations

Next, we describe the variability in the currents and water density decomposed into three distinct frequency bands: HF, MF and LF (they are defined in section 2.2).

At the KeN station, the HF band contained more kinetic energy than the MF band in the layer from 8 to 70 meters. In the layer from 20 to 65 meters, the LF energy predominated, possibly due to strong currents along the thalweg (Fig. 6a). Below 70 meters, kinetic energy consistently decreased for all three frequency bands. In general, the squared vertical shear of the HF band current velocity dominated over both the MF and LF bands in the upper 70 m layer. However, there were two exceptions, namely, in the 5 m layer centred at 45 m and in the 10 m layer centred at 65 m, the squared LF shear exceeded the squared shear of the HF band (Fig. 6b), probably due to the strong LF current in the layer 45 to 65 meters. Below 70 meters, the shear squared continuously decreased. The squared density fluctuations ( $\sigma_0'^2$ ) for HF and LF bands showed a maximum in the layer from 10 to 20 meters, with the LF signal exceeding the HF signal approximately fourfold (Fig. 6c). The MF band  $\sigma_0'^2$  exceeded the HF band signal only in the upper 10 meters. All three frequency band signals exhibited a second maximum in the layer between 40 and 70 meters, although weaker than in the upper layer.

At the KeS station, the MF and LF band kinetic energies were approximately equal, both being twice as small as the HF band kinetic energy (Fig. 6d). Only the MF band signal displayed slightly elevated values in a 10-meter-thick layer centred at 30 meters depth. The MF and LF band current vertical shear squared had very low values throughout the water column. In contrast, the HF band shear squared exhibited values similar to the mid-depth values at the KeN station (Fig. 6e). The HF and MF bands of  $\sigma_0'^2$  showed a similar vertical structure and values, with values increasing below 20 meters depth. The LF band signal had values about ten times larger and increased with depth below 20 meters (Fig. 6f).

Since kinetic energy and shear square in the submesoscale band (which largely coincides with the HF band) predominantly (outside of strong current events and related elevated shear) exceeded those parameters in other frequency bands, then below, a more detailed analysis of this frequency band is given. In addition to the HF frequency range, we use a BLF (broad LF)

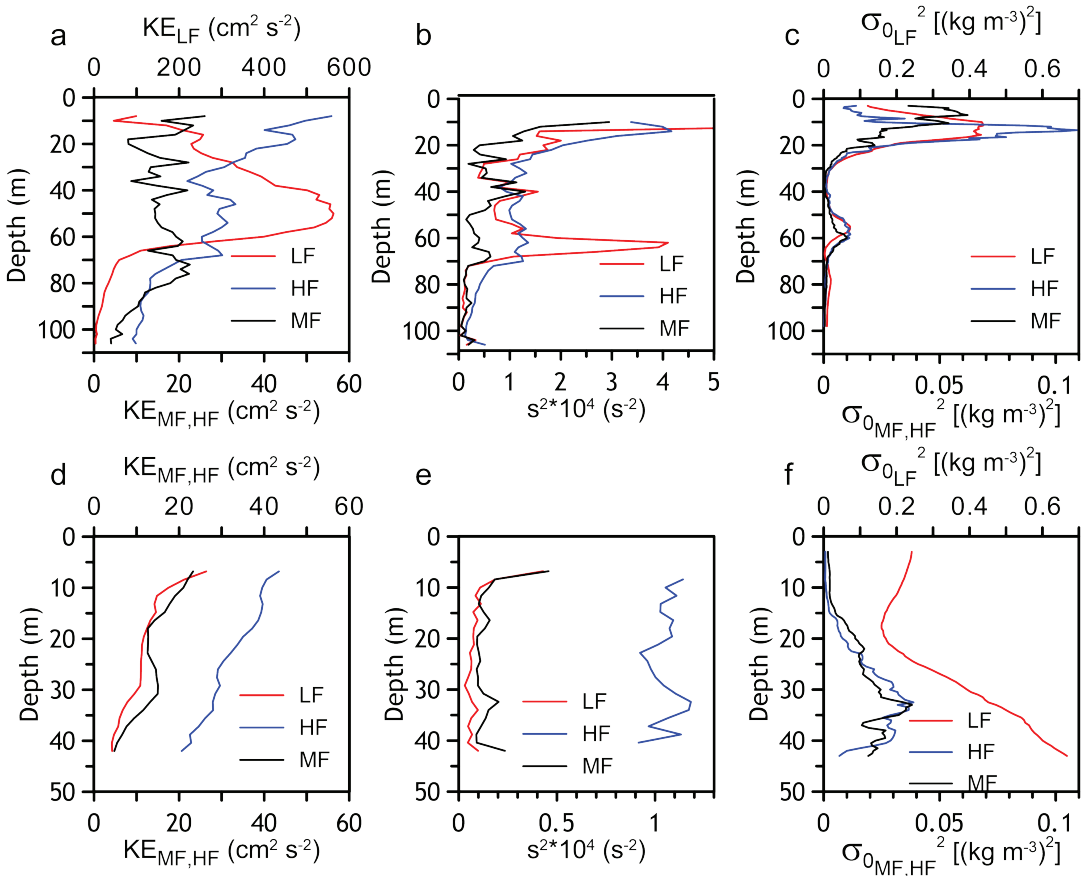


**Fig 6.** Time-averaged vertical profiles of kinetic energy, current velocity vertical shear squared, and density fluctuations squared for timescales < 36h, 36–168h and > 168h at measurement stations KeN (upper panel) and KeS (lower panel). At KeN measuring station, the time-averaging period for current velocity data was 26.07–17.08 (3 weeks) and for water density data 02.08–17.08 (2 weeks). At the KeS station, the time-averaging period was 28.08–02.10 (5 weeks) for both velocity and water density data.

range in the text below. The BLF range is the sum of the MF and LF ranges above.

### High-frequency (submesoscale) variability

#### High-frequency (submesoscale) variability at depth coordinates

In the KeN station, the absence of continuous CTD measurements in the upper layer during the first week of the three-week observation period precluded the analysis of small-scale temperature and salinity fluctuations. Instead, we derived temperature and density fluctuations ( $T'$  and  $\sigma_0'$

products) for the subsequent two weeks of measurements using high pass filtering with a cutoff timescale of 36 hours.

Analysis of the time series of  $\sigma_0'$  and  $T'$  standard deviations and minimum and maximum values at depth coordinates revealed elevated values within the upper 30 meters (within the thermocline) and the layer from 50 to 60 meters (within the halocline). Specifically, the thermocline exhibited minimum and maximum  $\sigma_0'$  values of  $-1.5$  and  $1.4$   $kg m^{-3}$ , respectively. The standard deviation of  $\sigma_0'$  in the thermocline was  $0.3$   $kg m^{-3}$ , whereas, in the halocline, it was  $0.1$   $kg m^{-3}$ . The temperature fluctuations corresponding to these values were  $6.2$  and  $-5.0^\circ C$  and  $1.5$  and  $0.2^\circ C$ , respectively (Fig. 7a, b).

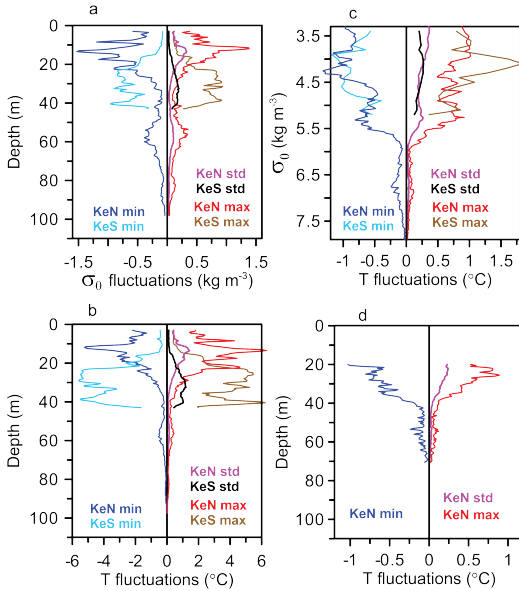


**Fig 7.** Vertical distributions of min, max and std of HF fluctuations of water density (a) and temperature (b) at KeN and KeS stations during CTD measurement periods, and HF temperature min, max, and std deviation as a function of  $\sigma_0'$  (c). (d) vertical profiles of min, max and std of HF temperature fluctuations at KeN station after removal of isopycnal vertical motions (free of IW contribution).

Similarly, at the KeS station,  $\sigma_0'$  values displayed minimum and maximum extremes within the thermocline (20 to 40 meters), reaching  $-1.0$  and  $0.9$  kg m<sup>-3</sup>, respectively. The standard deviation of  $\sigma_0'$  within the thermocline was approximately  $0.2$  kg m<sup>-3</sup>. The temperature fluctuations corresponding to these values were  $6.2$  and  $-5.5^\circ\text{C}$  and  $1.2^\circ\text{C}$ , respectively (Fig. 7a, b).

### High-frequency (submesoscale) variability at isopycnal surfaces

The observed variability in density and temperature at a specific depth can arise from vertical and horizontal movements of water masses with distinct temperature ( $T$ ) and salinity ( $S$ ) characteristics or from vertical mixing. To isolate submesoscale (SMS) temperature and salinity fluctuations in the high-frequency band, free from the influence of vertical movements and oscillations, we present temperature ( $T'$ ) and salinity fluctuations ( $S'$ ) at isopycnals. This approach reveals fluctuations due to temperature and salinity variability at isopycnal surfaces or diapycnal mixing.

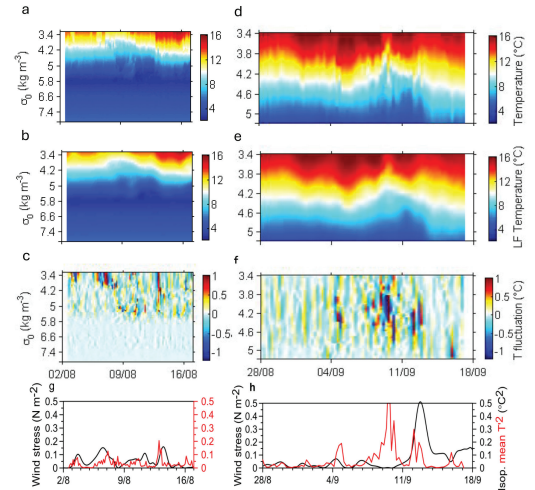


**Fig 8.** Measured temperature, low-passed filtered (cutoff 36h) temperature, and HF temperature fluctuations at isopycnal surfaces at KeN station (left column; a, b, and c, respectively) and KeS station (right column; d, e, and f, respectively). The relationship between wind stress and the strength of SMS processes (the mean value of the squares of the temperature fluctuations over the measured density range) is shown at KeN and KeS stations (g) and (h), respectively.

At the KeN station, temporal variability of temperature and salinity occurred at both scales, HF and LF (cutoff 36h), at densities ( $\sigma_0$ )  $< 5.5$  kg m<sup>-3</sup> (refer to Fig. 8a and b). Notably, in the uppermost layer (up to  $4.5$  kg m<sup>-3</sup>) during the second week of measurements (on 6 August), strong HF  $T'$  fluctuations were observed, indicating the presence of SMS footprints (Fig. 8c).

A similar patch of  $T'$  variability was identified in deeper layers at densities  $> 5$  kg m<sup>-3</sup> during the third week, aligning with the second strongest wind event near the end of the CTD measurement period (on 13 August) (Fig. 8c). Specifically, a low-temperature water mass, compensated by a decrease in salinity, arrived on 7 August, persisting for four days. Subsequently, from 12 August to 17 August, a warmer water mass, compensated by a salinity increase, replaced the colder one (Fig. 8b). These movements of water masses resulted in significant negative and positive values of  $T'$  at isopycnal surfaces  $< 5.5$  kg m<sup>-3</sup> (Fig. 8c). The minimum

fluctuations ( $S'$ ) at isopycnals. This approach reveals fluctuations due to temperature and salinity variability at isopycnal surfaces or diapycnal mixing.

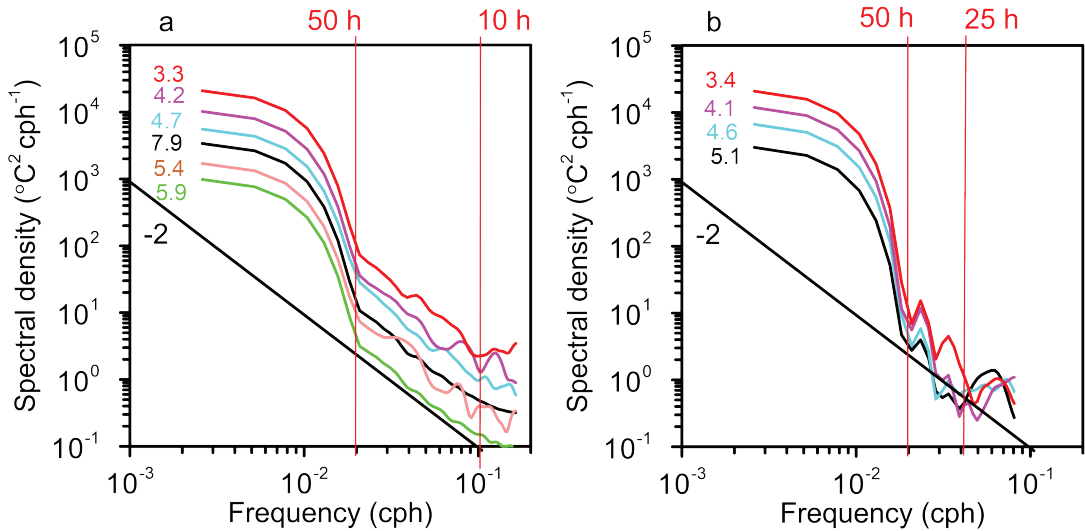


**Fig 9.** (a) KeN station, isopycnal temperature spectral density at isopycnals 3.3 (surface) to 7.9 (bottom) (the spectra have 8 degrees of freedom (dof)); (b) KeS station, isopycnal temperature spectral density at isopycnals 3.4 (surface) to 5.1 (bottom) (dof = 8) (the interval between red lines shows the time scales with approximate spectral slope  $-2$ ).

and maximum values of HF temperature fluctuations were approximately between  $-1$  and  $1^\circ\text{C}$  (Fig. 7c).

At the KeS station, temperature variability in HF and LF scales occurred throughout the entire density range (Fig. 8d and e). At  $\sigma_0$  isosurfaces from  $3.8$  to  $4.5 \text{ kg m}^{-3}$ , quasi-single negative and positive  $T'$  events appeared in the middle of downwelling relaxation on 4 September (Fig. 8f). Three days later, a series of negative and positive  $T'$  occurred for almost three days in a wide density range ( $3.6$  to  $4.8 \text{ kg m}^{-3}$ ).

Following strong wind events on 12 and 13 September, elevated  $T'$  values were observed within a density range from  $4.0$  to  $4.7 \text{ kg m}^{-3}$  (Fig. 8f). The minimum and maximum  $T'$  values ( $-1.2$  and  $1.8^\circ\text{C}$ , respectively) appeared in the layer at densities about  $4 \text{ kg m}^{-3}$  (Fig. 7c).

A comparison of HF  $T'$  fluctuations with the wind stress (Fig. 8g and h) shows that the elevated submesoscale variability can be related to strong wind events as well as occur in relatively calm weather conditions. For instance, the largest HF temperature variations on isopycnal surfaces were observed after the downwelling relaxation in calm conditions at KeS on 9 September (after a moderate and short-time opposing wind event; see Figs. 8h and 4a).

To ascertain that the observed temperature fluctuations at isopycnal surfaces were indicative of SMS processes, we analysed the spectra of isopycnal temperature fluctuations. At the KeN station, the spectrum slope followed  $-2$  at scales of 10 to 50 hours, characteristic of SMS processes (Fig. 9a) from the surface to the bottom (at a density range of  $3.3$  to  $7.9 \text{ kg m}^{-3}$ ). Similarly, at the KeS station (Fig. 9b), the spectrum slope followed approximately  $-2$  at scales of 25 to 50 hours in the entire water column (at a density range of  $3.4$  to  $5.1 \text{ kg m}^{-3}$ ). We suggest that the observed fluctuations signify SMS processes within these time scales. This topic will be discussed in the Discussion section.

**From isopycnal temperature fluctuations back to depth coordinate (IW free HF signal)**

Moving to  $\sigma_0$  coordinates reduced the  $T'$  min/max and std values as expected, as the contribution of internal waves (in HF band IW marks the contribution of seiches, tides, and quasi-inertial waves to the vertical movements of isopycnals) in  $T'$  was removed. Next, we transform the HF isopycnal  $T'$  back to the depth coordinate. Relat-

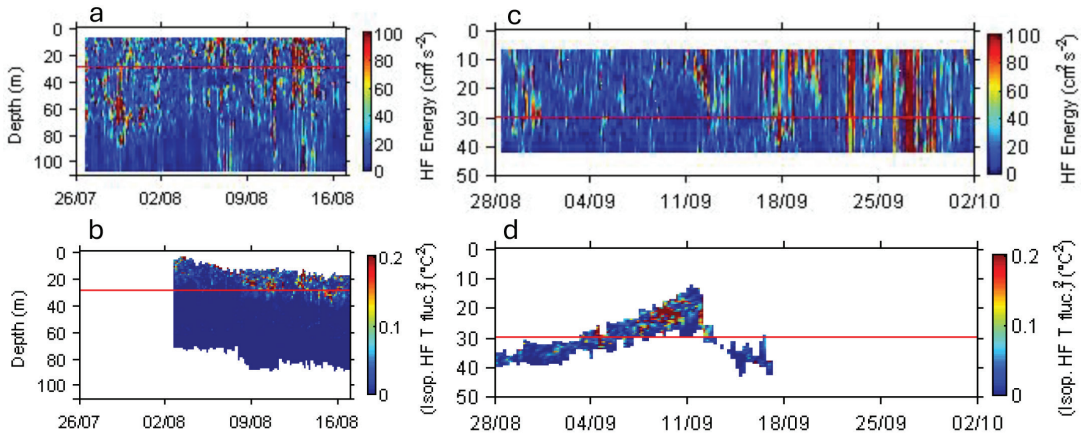


**Fig 10.** High frequency (cutoff 36 h) current velocity kinetic energy and water temperature fluctuation squared (only SMS contribution remained) at KeN and KeS stations (**a, b** and **c, d**, respectively, with a pink line the 30 m depth is marked for better tracking).

ing depth to  $T'$  observed at  $\sigma_0$  isolines allowed an estimation of the IW contribution to the HF variability in temperature. At the KeN station, in the ten-meter layer (from 20 to 30 meters), where IW-free  $T'$  data with high values were observed (Fig. 7d), the layer mean standard deviation decreased from 0.51 to 0.21°C, accounting for 41% of the initial value. In an extended layer (from 20 to 40 meters), the layer mean standard deviation decreased from 0.33 to 0.16°C, making 48% of the initial value. Therefore, approximately 50% of HF variability arises from SMS processes, while the remaining 50% stems from isopycnal vertical excursions (IW contribution).

Additionally, converting  $T'$  from  $\sigma_0$  coordinates to depth enables a rough estimate of the co-appearance of peak isopycnal temperature fluctuations with peak kinetic energy values (Fig. 10). At the KeN station, time-depth patches with high  $T'$  square values in the upper layer to 35 meters mostly coincided with high HF kinetic energy values. However, HF kinetic energy patches were observed in a wide range of depths and dates, with rare occurrences below 70 meters. In the KeS station, co-appearance is evident on 4 September at a depth interval of 30–35 meters and on 12 September at depths of 15 to 25 meters. Notably, a distinguishable patch in the layer from 20 to 25 meters on 9 September did not reveal an analogous patch in kinetic energy.

## Discussion

In the Gulf of Finland, the substantial runoff from the Neva River in the east and unrestricted water exchange with the northern Baltic proper in the west creates horizontal density gradients (e.g. Alenius *et al.* 1998, Leppäranta and Myrberg 2009). In addition, mesoscale phenomena, such as eddies and wind-driven upwellings/downwellings, frequent in the gulf, contribute to the formation of sharp density and current velocity gradients. These conditions provide a conducive environment for submesoscale (SMS) processes to develop, influencing vertical mixing and restratification and contributing to the variability of oceanographic fields at spatial scales less than mesoscale (Lips *et al.* 2016, Väli *et al.* 2017).

We analysed simultaneous time-series data of vertical profiles of temperature, salinity, and current velocity collected at a deep station on the thalweg near Keri Island over three weeks and at a shallow station outside the thalweg over five weeks. The goal was to identify the events of active SMS processes within the context of large- and mesoscale phenomena.

The obtained time series were divided into broad low-frequency (timescales greater than 36 hours) and high-frequency (timescales less than 36 hours) bands, based on the observed energy spectrum minimum visible at the 36-hour timescale. This division allowed us to study

SMS processes separately from more energetic low-frequency phenomena. Based on the modelling and measurements, previous studies have shown that about 75% of energy in the Gulf of Finland belongs to the broad low-frequency band (including mesoscale) (Laanemets *et al.* 2011; Lilover *et al.* 2011). The high-frequency band, explaining about 25% of energy, consists not only of SMS currents but also currents initiated by tides, seiches, and inertial oscillations.

Consistent with previous observations (e.g., Suhhova *et al.* 2018), we found that low-frequency currents in the upper layer were directed toward the wind vector, while in the layer below, the flow was directed against the wind vector. However, the upper layer currents could not be measured during the upwelling along the southern coast, as the uppermost layers were beyond the ADCP's measurement range. In the cold intermediate layer (ranging from 20 to 60 meters, e.g. Liblik and Lips 2011), we observed extremely high eastward velocities up to 70 cm s<sup>-1</sup>, directed against the wind vector during the upwelling period. These currents likely compensated the westward upper layer flow produced by successive easterly wind events; it ceased when the wind changed direction. Currents in the bottom layer (below 80 meters) did not exhibit high values until a very strong wind event on 12 September; after this, the bottom currents also reached relatively high values of 25 cm s<sup>-1</sup>, which lasted periodically for about two weeks until 28 September. The high kinetic energy close to the bottom and the oscillation period of about five days suggest the presence of topographic waves (Talpsepp 2006).

During the first week of measurements at the deep thalweg station, a strong easterly wind impulse triggered a typical upwelling situation along the southern coast. Over the following two weeks, due to prevailing westerly winds, upwelling relaxation occurred, and towards the end of the measurement period, a downwelling had developed, leading to the warming and thickening of the upper mixed layer. Temperature fluctuations in time at the submesoscale (less than 36 hours) intensified in the thermocline (10–20 meters depth) during downwelling-supporting westerly wind events and during the upwelling relaxation period. These fluctuations

coincided with changes in the velocity and water density. It aligns with the high-resolution modelling study by Väli *et al.* (2017), which showed the formation of high vorticity eddies during the upwelling relaxation phase. By the end of the third week, the 15-degree temperature isoline, approximately marking the centre of the thermocline, had descended to a depth of 20 meters. Temperature fluctuations followed this descent, indicating the strong connection between submesoscale variability and background mesoscale phenomena.

Eleven days later, at a nearby shallow station (46 meters deep, 2.5 km southeast), the downwelling relaxation occurred during two weeks of calm weather with the 15-degree temperature isoline rising from 35 meters to 15 meters. Subsequently, downwelling was maintained and evolved over three weeks by a series of stormy wind events.

To study the evolution of SMS signal variability, we excluded the contribution of internal waves to the SMS signal by analysing temperature and salinity at isopycnal surfaces. For instance, at the beginning of the downwelling relaxation period, the observed high-value patch of temperature fluctuations in the 25 to 35-meter depth interval disappeared when moving to the sigma coordinates, suggesting fluctuations were due to vertical movements. In the middle of the downwelling relaxation, successive positive and negative temperature fluctuations were observed over three days on the isopycnal surfaces, which we interpreted as the footprints of SMS processes across a wide range of densities (1003.6 to 1004.8 kg m<sup>-3</sup>, roughly corresponding to 25–33 meters depth). Similarly, strong successive positive and negative temperature fluctuations were noted on the density isolines during the upwelling relaxation period at the thalweg station.

These temperature and salinity fluctuations could be attributed to submesoscale vortices or spiral eddies formed during the relaxation phase, as suggested by numerical model studies. Earlier reports by Laanemets *et al.* (2011), Väli *et al.* (2017) and Liblik *et al.* (2020) indicated intensive squirts, eddies, and vortices in the coastal zones of the Gulf of Finland. The presence of SMS processes was confirmed by the

–2 spectrum slope of water temperature variance at the isopycnal surfaces observed at the deep station throughout the entire water column for time scales of 10 to 50 hours. Similarly, a spectrum slope of about –2 at time scales of 25 to 50 hours was observed at the shallow station. The –2 spectrum slope of tracer variance in the wavenumber domain was previously reported in the thermocline using glider observations by Salm *et al.* (2023). Such a steeper slope than predicted by quasi-geostrophic turbulence theory has also been observed in other regions (e.g. Cole and Rudnick 2012) and suggested to be characteristic of submesoscale processes (Jaeger *et al.* 2020). This suggestion holds for our analysis in the frequency domain if assuming a frozen flow-field approximation (Balwada *et al.* 2024).

The distribution of observed temperature variability between SMS and oscillating processes revealed that approximately 50% of the total temperature fluctuations in the HF range (SMS range) were explained by SMS processes. These fluctuations were significant, ranging from –1.2 to 1.0 °C at the thalweg station and from –1.2 to 1.8 °C at the shallow water station, confirming the important impact of SMS processes on the horizontal and vertical exchanges in the upper layer of the sea.

The observed co-occurrence of peak current velocity kinetic energy and temperature/density fluctuations suggests geostrophically balanced SMS processes. The probable mechanisms of the development of SMS processes could include Mixed Layer Instability (MLI) and Symmetric Instability (SI). Using high-resolution modelling, Zhurbas *et al.* (2021) found that classic symmetric instability and strain-induced frontogenesis likely contribute to the formation of submesoscale striped textures in the surface layer of the northeastern Baltic Proper. However, due to the lack of data on current velocity and buoyancy horizontal gradients, we cannot definitively determine the specific SMS processes taking place; we can only confirm the presence of SMS variability in the observations.

In the past, submesoscale structures in the Baltic Sea have primarily been studied through modelling and remote sensing, with fewer *in situ* measurements of thermohaline fields (Carpenter *et al.* 2020; Salm *et al.* 2023). Our analysis,

based on point measurements of temperature, salinity, and velocity fields in the Gulf of Finland, revealed the presence of submesoscale variability "footprints" in the region. The physical background in our study area (presence of horizontal buoyancy gradients, frequent upwelling/downwelling events, mesoscale fronts) favours the appearance of submesoscale processes (Salm *et al.* 2023; Väli *et al.* 2024), and we suggest that similar submesoscale activity can occur in other stratified sea areas. To identify different submesoscale processes from measurements and determine their origin and characteristic features in the Gulf of Finland and similar sea areas, it is necessary to conduct high-resolution measurements in time and space by combining point measurement and the glider or Scanfish surveys.

## Conclusions

- 1) Upwelling and downwelling relaxation periods revealed high-frequency temperature (density) fluctuations throughout the upper part of the water column, coinciding with changes in velocity and salinity.
- 2) The spectrum slope –2 of temperature variance at isopycnal surfaces confirmed the presence and dominance of submesoscale processes in the entire water column at time scales up to 50 hours.
- 3) Temperature fluctuations caused by submesoscale processes at isopycnals ranged from one to two degrees (°C), constituting approximately 50% of high-frequency variability, with the remaining 50% attributed to isopycnal vertical excursions (contribution of internal waves).
- 4) The frequent presence of submesoscale processes in the Gulf of Finland dynamics is crucial in forming layered vertical distributions of density and currents.
- 5) For a comprehensive understanding, high-resolution measurements in time and space conducted with gliders and profilers are necessary to identify and characterize the various submesoscale processes in the Gulf of Finland

*Acknowledgements:* This work was supported by the Estonian Research Council grant (PRG602).

## References

- Alenius P., Myrberg K., & Nekrasov A. 1998. The physical oceanography of the Gulf of Finland: a review. *Boreal Env. Res.* 3(2): 97–125.
- Balwada, D., Gray, A. R., Dove, L. A., & Thompson, A. F. 2024. Tracer stirring and variability in the Antarctic Circumpolar Current near the Southwest Indian Ridge. *Journal of Geophysical Research: Oceans* 129(1): e2023JC019811.
- Burchard H., Basdurak N. B., Gräwe U., Knoll M., Mohrholz V., & Müller S. 2017. Salinity inversions in the thermocline under upwelling favorable winds. *Geophysical Research Letters* 44(3): 1422–1428.
- Callies J., Barkan R., & Garabato A. N. 2020. Time scales of submesoscale flow inferred from a mooring array. *Journal of Physical Oceanography* 50(4): 1065–1086.
- Capet X., McWilliams J. C., Molemaker M. J., & Shchepetkin A. F. 2008. Mesoscale to submesoscale transition in the California Current System. Part I: Flow structure, eddy flux, and observational tests. *Journal of Physical Oceanography* 38(1): 29–43.
- Carpenter, J. R., Rodrigues, A., Schultze, L. K., Merkelbach, L. M., Suzuki, N., Baschek, B., & Umlauf, L. 2020. Shear instability and turbulence within a submesoscale front following a storm. *Geophysical Research Letters* 47(23): e2020GL090365.
- Chrysagi, E., Umlauf, L., Holtermann, P., Klingbeil, K., & Burchard, H. 2021. High-resolution simulations of submesoscale processes in the Baltic Sea: The role of storm events. *Journal of Geophysical Research: Oceans* 126(3): e2020JC016411.
- Cole, S. T., & Rudnick, D. L. 2012. The spatial distribution and annual cycle of upper ocean thermohaline structure. *Journal of Geophysical Research: Oceans* 117(C2).
- Gill A. E., Green J. S. A., & Simmons A. J. 1974. Energy partition in the large-scale ocean circulation and the production of mid-ocean eddies. *Deep sea research and oceanographic abstracts* 21(7): 499–528.
- Gula J., Molemaker M. J., & McWilliams J. C. 2014. Submesoscale cold filaments in the Gulf Stream. *Journal of Physical Oceanography* 44(10): 2617–2643.
- Gurova E., & Chubarenko B. 2012. Remote-sensing observations of coastal sub-mesoscale eddies in the south-eastern Baltic. *Oceanologia* 54(4): 631–654.
- Haapala J., & Alenius P. 1994. Temperature and salinity statistics for the northern Baltic Sea 1961–1990. *Finnish Mar. Res.* 262: 51–121.
- Jaeger, G. S., MacKinnon, J. A., Lucas, A. J., Shroyer, E., Nash, J., Tandon, A., Farrar, J. T. & Mahadevan, A. 2020. How spice is stirred in the Bay of Bengal. *Journal of Physical Oceanography* 50(9): 2669–2688.
- Karimova S., & Gade M. 2016. Improved statistics of sub-mesoscale eddies in the Baltic Sea retrieved from SAR imagery. *International Journal of Remote Sensing* 37(10): 2394–2414.
- Laanemets J., Väli G., Zhurbas V., Elken J., Lips I., & Lips U. 2011. Simulation of mesoscale structures and nutrient transport during summer upwelling events in the Gulf of Finland in 2006. *Boreal Env. Res.* 16A: 15–26.
- Leppäranta M., & Myrberg K. 2009. *Physical oceanography of the Baltic Sea*. Springer Science & Business Media.
- Lévy M., Franks P. J., & Smith K. S. 2018. The role of submesoscale currents in structuring marine ecosystems. *Nature communications* 9(1), 4758.
- Liblik T., & Lips U. 2011. Characteristics and variability of the vertical thermohaline structure in the Gulf of Finland in summer. *Boreal Env. Res.* 16A: 73–83.
- Liblik T., & Lips U. 2012. Variability of synoptic-scale quasi-stationary thermohaline stratification patterns in the Gulf of Finland in summer 2009. *Ocean Science* 8(4): 603–614.
- Liblik, T., Väli, G., Lips, I., Lilover, M. J., Kikas, V., & Laanemets, J. 2020. The winter stratification phenomenon and its consequences in the Gulf of Finland, Baltic Sea. *Ocean Science* 16(6): 1475–1490.
- Lilover M. J., Pavelson J., & Kõuts T. 2011. Wind forced currents over the shallow Naissaar Bank in the Gulf of Finland. *Boreal Env. Res.* 16: 164–174.
- Lilover M. J., Elken J., Suhhova I., & Liblik T. 2017. Observed flow variability along the thalweg, and on the coastal slopes of the Gulf of Finland, Baltic Sea. *Estuarine, Coastal and Shelf Science* 195: 23–33.
- Lips U., Kikas V., Liblik T., & Lips I. 2016. Multi-sensor in situ observations to resolve the sub-mesoscale features in the stratified Gulf of Finland, Baltic Sea. *Ocean Science* 12(3): 715–732.
- McWilliams J. C. 2016. Submesoscale currents in the ocean. *Proceedings of the Royal Society A: Mathematical, Physical and Engineering Sciences* 472(2189), 20160117.
- Molemaker M. J., McWilliams J. C., & Capet X. 2010. Balanced and unbalanced routes to dissipation in an equilibrated Eady flow. *Journal of Fluid Mechanics* 654: 35–63.
- Pietri A., Testor P., Echevin V., Chaigneau A., Mortier L., Eldin G., & Grados C. 2013. Finescale vertical structure of the upwelling system off southern Peru as observed from glider data. *Journal of Physical Oceanography* 43(3): 631–646.
- Salm K., Liblik T., & Lips U. 2023. Submesoscale variability in a mesoscale front captured by a glider mission in the Gulf of Finland, Baltic Sea. *Frontiers in Marine Science* 10, 984246.
- Suhhova I., Liblik T., Lilover M. J., & Lips U. 2018. A descriptive analysis of the linkage between the vertical stratification and current oscillations in the Gulf of Finland. *Boreal Env. Res.* 23: 83–103.
- Sullivan P. P., & McWilliams, J. C. 2018. Frontogenesis and frontal arrest of a dense filament in the oceanic surface boundary layer. *Journal of Fluid Mechanics* 837: 341–380.
- Talpssepp L. 2006. Periodic variability of currents induced by topographically trapped waves in the coastal zone in the Gulf of Finland. *Oceanologia* 48(S): 75–90.
- Tavri A., Singha S., Lehner S., & Topouzelis K. 2016. Observation of sub-mesoscale eddies over Baltic Sea using TerraSAR-X and Oceanographic data. In *Proceedings of Living Planet Symposium*.

- Thomas L. N., Tandon A., & Mahadevan A. 2008. Submesoscale processes and dynamics. *Ocean Modeling in an Eddy Regime* 177: 17–38.
- Thomas L. N., Taylor J. R., Ferrari R., & Joyce T. M. 2013. Symmetric instability in the Gulf Stream. *Deep Sea Research Part II: Topical Studies in Oceanography* 91: 96–110.
- Thompson A. F., Lazar A., Buckingham C., Garabato A. C. N., Damerell G. M., & Heywood K. J. 2016. Open-ocean submesoscale motions: A full seasonal cycle of mixed layer instabilities from gliders. *Journal of Physical Oceanography* 46(4): 1285–1307.
- Väli G., Zhurbas V., Lips U., & Laanemets J. 2017. Submesoscale structures related to upwelling events in the Gulf of Finland, Baltic Sea (numerical experiments). *Journal of Marine Systems* 171: 31–42.
- Väli G., Zhurbas V. M., Laanemets J., & Lips U. 2018. Clustering of floating particles due to submesoscale dynamics: a simulation study for the Gulf of Finland, Baltic Sea. *Фундаментальная и прикладная гидрофизика* 11(2): 21–35.
- Väli G., Meier H. M., Liblik T., Radtke H., Klingbeil K., Gräwe U., & Lips U. 2024. Submesoscale processes in the surface layer of the central Baltic Sea: A high-resolution modelling study. *Oceanologia* 66(1): 78–90.
- Zhang Y., Dong C., Chen X., & Wang Y. 2020. Observation of submesoscale turbulence in a cyclonic eddy. *Ocean Dynamics* 70(4): 513–520.
- Zhurbas V., Väli G., & Kuzmina N. 2021. Striped texture of submesoscale fields in the northeastern Baltic Proper: Results of very high-resolution modelling for summer season. *Oceanologia* 64(1): 1–21.